ISSN 1070-3284, Russian Journal of Coordination Chemistry, 2020, Vol. 46, No. 11, pp. 746–755. © Pleiades Publishing, Ltd., 2020.
Russian Text © The Author(s), 2020, published in Koordinatsionnaya Khimiya, 2020, Vol. 46, No. 11, pp. 672–681.

Specific Features of EPR Spectroscopy of Organotin Compounds with Paramagnetic Ligands of the *o*-Iminobenzosemiquinone Type

M. G. Chegerev[a], K. V. Arsenyeva[b], A. V. Cherkasov[b], and A. V. Piskunov[b, *]

[a] *Research Institute of Physical and Organic Chemistry, Southern Federal University, Rostov-on-Don, Russia*
[b] *Razuvaev Institute of Organometallic Chemistry, Russian Academy of Sciences, Nizhny Novgorod, 603600 Russia*
**e-mail: pial@iomc.ras.ru*

Received May 5, 2020; revised June 5, 2020; accepted June 10, 2020

Abstract—New paramagnetic tin(IV) derivatives containing the radical-anion of 2,4,6,8-tetra-*tert*-butylphenoxazin-1-one redox-active ligand (phenox-imQ) are synthesized and studied by EPR spectroscopy. Complexes **I**–**V** are paramagnetic in the crystalline state and in solution. The geometry of the obtained paramagnetic species and spin density distribution in them are studied by the Density functional theory. Diamagnetic complex **VI** is synthesized from the phenox-imQ dianion, and its one-electron oxidation is studied. The molecular structure of complex **VI** · THF is determined by X-ray diffraction analysis (CIF file CCDC no. 2000962 (**VI** · THF)).

Keywords: phenoxazin-1-one, redox-active ligand, tin, EPR, coordination polyhedron
DOI: 10.1134/S1070328420110019

INTRODUCTION

The chemistry of redox-active ligands is being developed during the recent 50 years. When just discovered, similar ligands and their metal complexes were objects of EPR spectroscopic studies only [1]. However, the true potential of these ligands turned out to be much wider, and at present they are unique tools for the extension of the reactivity of both transition and main-group metal complexes. The use of the derivatives of the redox-active ligands in the coordination and organoelement chemistry of metals made it possible to accomplish transformations that earlier considered to be unfeasible: the facilitation of redox reactions of the *s*-, *p*-, and *d*-metal derivatives; cross-coupling reactions without a change in the oxidation state of the metallocenter; and a phenomenon of redox isomerism and its practical use [2–8].

At the moment, many works devoted to the synthesis and study of the structures and catalytic or magnetic properties of the transition metal complexes based on redox-active ligands of various nature, *o*-quinones (Q), *o*-iminoquinones (imQ), α-diimines (DAD), and their substituted analogs, have been published [9–11]. The introduction of the radical-anionic (*o*-semiquinone, SQ) ligand into metal complexes provides opportunities for studying the dynamics of the coordination sphere of the complex-forming agent in situ using EPR spectroscopy. Unpaired electron localized on the paramagnetic ligand exerts no appreciable effect on the metal and its environment. This feature means that *o*-semiquinones can be used as spin labels. The parameters of the EPR spectra of the semiquinone complexes (*g* factor, hyperfine structure, and hyperfine coupling (HFC) constants) are very sensitive to the nature of the metal atom, ligand environment and geometric configuration of the complex [12–17].

Although *o*-iminoquinones [18, 19] are the closest structural analogs of *o*-quinones, they differ noticeably in chemistry. In particular, this fact is distinctly seen for the chemistry of Group 14 elements (Si, Ge, Sn, Pb) with the above listed redox-active ligands. The *o*-semiquinone compounds of the silicon subgroup elements are poorly stable, and the paramagnetic species rapidly decompose in solutions via two most probable mechanisms: the disproportionation of the *o*-semiquinone complex or elimination of the hydrocarbon radical (R) at the metal atom of the complex-forming agent. The ratio of these two processes depends on the nature of the metal, quinone ligand, and hydrocarbon substituent [20–22]. At the same time, the use of *o*-iminoquinones made it possible to isolate and structurally characterize many stable paramagnetic derivatives of the general type $imSQMX_3$, where imSQ is the radical anion of *o*-iminobenzoquinone; and X is alkyl, aryl, or halogen [23, 24].

This work is devoted to the synthesis of new tin(IV) compounds based on redox-active 2,4,6,8-tetra-*tert*-butylphenoxazin-1-one (phenox-imQ) and to the study of the physicochemical properties of the synthesized compounds. Since the considered substituted phenoxazinone is bidentate *o*-iminoquinone, we examined the synthesized tin(IV) complexes in comparison with the earlier known tin compounds based

on *N*-aryl-substituted *o*-iminoquinones. The study of the compounds of a similar class would make it possible to extend concepts on the structures, character of binding, and spin density distribution in the tin *o*-iminoquinone derivatives depending on the structure of the redox-active ligand.

EXPERIMENTAL

All procedures on the synthesis of the tin phenoxazinone complexes and their chemical transformations were carried out in the absence of air oxygen and moisture. The solvents used in the work were purified and dehydrated using standard procedures [25].

IR spectra were recorded on an FSM-1201 FT-IR spectrometer in a range of 450–4000 cm^{-1} in Nujol in KBr cells. Elemental analysis was carried out on an Elementar Vario El cube analyzer. EPR spectra were recorded on a Bruker-EMX spectrometer (working frequency ~9.7 GHz). Diphenylpicrylhydrazyl (g_i = 2.0037) was used as a standard for the determination of the *g* factor. EPR spectra were simulated using the Easyspin program package for Matlab [26].

Synthesis of redox-active phenox-imQ was carried out using an original procedure which is a modification of published earlier [27]. 4,6-Di-*tert*-butyl-*o*-aminophenol (3.50 g, 15.8 mmol) [28] and 3,5-di-*tert*-butyl-*o*-benzoquinone (3.47 g, 15.8 mmol) were placed in a flask with a stirrer and dissolved in methanol (50 mL). After dissolution the reaction mixture turned intensively violet. Pyridine (5 mL) was added to the resulting solution, and the reaction mixture was refluxed with an air reflux condenser for 2 h. The reaction afforded a mixture of the oxidized and reduced forms of phenox-imQ. The dropwise addition of water to the reaction mixture resulted in the precipitation of a dark blue substance. The dry residue was dissolved in Et_2O, and the solution was transferred to a separating funnel. A saturated aqueous solution of $K_3Fe(CN)_6$ (20 g) and KOH (1 g) was added to the obtained mixture. The resulting reaction mixture was vigorously shaken. The oxidation process was monitored by thin-layer chromatography (TLC) using a hexane–ethyl acetate (1 : 30) system as an eluent. The disappearance of one of two blue spots on the chromatogram served as the indication of the reaction end. The obtained product was crystallized from hexane at −18°C. The formed dark blue crystals of phenox-imQ were decanted from the mother liquor. The yield was 5.26 g (78%). The spectroscopic data of the synthesized compound correspond to the published data [27, 29].

Phenoxazin-1-one disodium salt (phenox-$APNa_2$) was synthesized by the direct reduction of phenox-imQ with sodium excess in tetrahydrofuran (THF). The reaction was accompanied by a change in the color of the solution from dark blue to light yellow. The resulting solution was used in situ. The monosodium salt (phenox-imSQNa) was synthesized by the reaction of phenox-$APNa_2$ with phenoxazin-1-one in a molar ratio of 1 : 1 in THF. The reaction was accompanied by a change in the solution color from yellow to brown.

Synthesis of tin(IV) complexes (I–V) (general procedure). A solution of monosodium salt phenox-imSQNa (1.0 mmol) in THF (20 mL) was slowly added to a solution of organotin halide (1.0 mmol) in the same solvent (10 mL) followed by a change in the color of the reaction mixture from brown to vinous-red. The resulting solution was stirred at room temperature for 30 min, after which the solvent was removed under reduced pressure. The residue was treated with hexane (20 mL) and filtered on a glass Schott filter no. 4. The hexane solution was evaporated to half a volume and slowly cooled to −18°C. The formed finely crystalline precipitates of the synthesized tin complexes were decanted from the mother liquor and dried under reduced pressure.

The yield of the phenox-imSQSnMe_2Cl complex (**I**) was 75%.

For $C_{30}H_{46}NO_2ClSn$

Anal. calcd., %	C, 59.38	H, 7.64	Cl, 5.84
Found, %	C, 59.57	H, 7.83	Cl, 5.76

IR (ν, cm^{-1}): 1597 m, 1534 s, 1479 s, 1412 s, 1390 w, 1360 s, 1344 w, 1300 w, 1285 w, 1275 w, 1255 s, 1246 s, 1206 m, 1187 w, 1124 w, 1076 s, 1050 s, 1015 m, 992 m, 956 w, 930 w, 916 w, 889 m, 858 m, 838 m, 813 w, 770 m, 745 m, 684 m, 645 m, 620 s, 587 w, 547m, 495 w.

The yield of the phenox-imSQSnEt_2Cl complex (**II**) was 81%.

For $C_{32}H_{50}NO_2ClSn$

Anal. calcd., %	C, 60.54	H, 7.94	Cl, 5.58
Found, %	C, 60.70	H, 8.16	Cl, 5.45

IR (ν, cm^{-1}): 1598 m, 1533 s, 1478 s, 1412 s, 1390 w, 1360 s, 1344 w, 1299 w, 1285 w, 1274 w, 1255 s, 1245 s, 1206 m, 1186 w, 1124 w, 1076 s, 1050 s, 1015 m, 992 m, 956 w, 930 w, 916 w, 889 m, 858 m, 838 m, 813 w, 767 m, 742 m, 684 m, 645 m, 620 s, 587 w, 527 w, 525 m, 498 w.

The yield of the phenox-imSQSn(*t*-Bu)$_2$Cl complex (**III**) was 76%.

For $C_{36}H_{58}NO_2ClSn$

Anal. calcd., %	C, 62.57	H, 8.46	Cl, 5.13
Found, %	C, 62.89	H, 8.60	Cl, 5.02

IR (ν, cm^{-1}): 1597 m, 1534 s, 1479 s, 1412 s, 1390 w, 1360 s, 1344 w, 1318 w, 1285 w, 1275 w, 1255 s, 1246 s, 1206 m, 1187 w, 1124 w, 1076 s, 1050 s, 1015 m, 992 m,

956 w, 930 w, 916 w, 889 m, 858 m, 838 m, 813 w, 770 s, 745 m, 684 m, 645 m, 620 s, 587 w, 547 m, 489 w.

The yield of the phenox-imSQSnPh$_2$Cl complex (**IV**) was 80%.

For $C_{40}H_{50}NO_2ClSn$

Anal. calcd., %	C, 65.72	H, 6.89	Cl, 4.85
Found, %	C, 65.99	H, 6.98	Cl, 4.73

IR (ν, cm^{-1}): 1597 m, 1534 s, 1479 s, 1412 s, 1390 w, 1360 s, 1344 w, 1285 w, 1275 w, 1246 s, 1206 m, 1187 w, 1124 w, 1076 s, 1050 s, 1018 w, 985 m, 956 w, 930 w, 916 w, 889 m, 858 m, 838 m, 813 w, 770 s, 733 s, 695 s, 645 m, 650 w, 640 m, 587 w, 547m, 492 w.

The yield of the phenox-imSQSnPh$_3$ complex (**V**) was 82%.

For $C_{46}H_{55}NO_2Sn$

Anal. calcd., %	C, 71.51	H, 7.18
Found, %	C, 71.72	H, 7.32

IR (ν, cm^{-1}): 1597 m, 1534 s, 1479 s, 1412 s, 1390 w, 1360 s, 1344 w, 1285 w, 1275 w, 1247 s, 1204 s, 1187 w, 1124 w, 1076 s, 1050 s, 1018 w, 992 s, 956 w, 931 w, 916 w, 889 m, 858 m, 838 m, 813 w, 770 s, 733 s, 695 s, 645 m, 651 w, 642 m, 587 w, 547m, 492 w.

Synthesis of phenox-APSnEt$_2$ · THF complex (VI). A solution of phenox-APNa$_2$ (1.0 mmol) in THF (20 mL) was slowly added to a solution of Et$_2$SnCl$_2$ (1.0 mmol) in the same solvent (10 mL), and the color of the reaction mixture changed from yellow to intensive orange. The resulting solution was stirred at room temperature for 10 min, after which the solvent was removed under reduced pressure. The residue was treated with hexane (20 mL) and filtered on a glass Schott filter no. 4. A hexane solution was evaporated to half a volume, after which the crystals of complex **VI** were isolated. The yield was 62%.

For $C_{36}H_{57}NO_3Sn$

Anal. calcd., %	C, 64.48	H, 8.57
Found, %	C, 64.77	H, 8.72

^{1}H NMR (C_6D_6, 20°C), δ, ppm: 7.24 (d, 1H, J = 2.2 Hz, H_{Ar}); 6.89 (s, 1H, H_{AP}); 6.69 (d, 1H, J = 2.2 Hz, H_{Ar}); 3.43 (m, 4H, α-CH_2(THF)); 1.67 (s, 9H, (*t*-Bu)); 1.64 (q, 4H, J = 7.5 Hz, –CH_2–); 1.58 (s, 9H, (*t*-Bu)); 1.35 (m, 4H, β-CH_2(THF)); 1.32, 1.30 (s, 9H, (*t*-Bu)); 1.24 (t, 6H, J = 7.5 Hz, –CH_3).

IR (ν, cm^{-1}): 1594 m, 1541 m, 1441 s, 1362 s, 1340 m, 1316 m, 1302 w, 1273 w, 1254 m, 1236 m, 1200 m, 1169 m, 1119 m, 1049 s, 1006 m, 986 w, 957 w, 914 w, 883 m, 866 w, 852 m, 837 m, 808 w, 766 w, 756 w, 740 m, 673 m, 652 m, 600 w, 540 w, 524 w.

Quantum-chemical calculations were performed using the Gaussian09 program package [30] by the density functional theory (DFT) with the B3LYP functional [31] in the standard dgdzvp basis set for all atoms.

X-ray diffraction analysis (XRD) of a single crystal of complex **VI** · THF (0.40 × 0.40 × 0.10 mm) was carried out on a Rigaku OD Xcalibur diffractometer (ω scan mode, MoK_α radiation, λ = 0.71073 Å, T = 100(2) K, 2θ = 60.06°). The experimental sets of intensities were measured and integrated, absorption corrections were applied, and structure refinement was performed using the CrysAlisPro [32] and SHELX [33] program packages. Compound **VI** · THF ($C_{36}H_{57}NO_3Sn$ · C_4H_8O) crystallizes in the space group $P2_1/n$ (a = 14.9485(3), b = 16.3242(2), c = 17.8566(9) Å, β = 112.754(2)°, V = 4018.29(13) Å^3, Z = 4, ρ_{calc} = 1.108 g/cm^3, μ = 0.665 mm^{-1}). The number of measured reflections was 83764, and 11720 independent reflections (R_{int} = 0.0506) were used for the solution of the structure followed by the refinement of 383 parameters by full-matrix least squares for F^2_{hkl} in the anisotropic approximation for non-hydrogen atoms. The hydrogen atoms in complex **VI** · THF were placed in the geometrically calculated positions and refined isotropically with fixed thermal parameters $U(H)_{iso}$ = $1.2U(C)_{equiv}$ ($U(H)_{iso}$ = $1.5U(C)_{equiv}$ for methyl groups). The contribution of the solvate THF molecule to the structural model of complex **VI** · THF was taken into account using the SQUEEZE procedure (Platon) [34]. After the final refinement, wR_2 = 0.0915 and $S(F^2)$ = 1.038 for all reflections (R_1 = 0.0359 for all reflections satisfying the condition $I > 2\sigma(I)$). The residual electron density maximum and minimum were 2.59 and –0.83 e/Å^3, respectively.

The structure of complex **VI** · THF was deposited with the Cambridge Crystallographic Data Centre (CIF file CCDC no. 2000962; ccdc.cam.ac.uk/structures).

RESULTS AND DICUSSION

Several approaches to the synthesis of redox-active phenox-imQ were described, but all of them are characterized by fairly low yields of the target product [27, 29]. We modified the published procedure in order to increase the yield of the studied ligand by supplementing an additional stage of the oxidation of the reaction mixture by potassium ferrocyanide. The reflux of equimolar amounts of 4,6-di-*tert*-butyl-*o*-aminophenol and 3,5-di-*tert*-butyl-*o*-benzoquinone in methanol affords a mixture consisting of the desired phenox-imQ and its reduced form phenox-imSQH in a ratio of ~1 : 1. The subsequent oxidation of the reaction mixture without isolation with potassium hexacyanoferrate(III) in an alkaline medium made it possible to increase the yield of the final product phenox-imQ twice as much (78%) (Scheme 1).

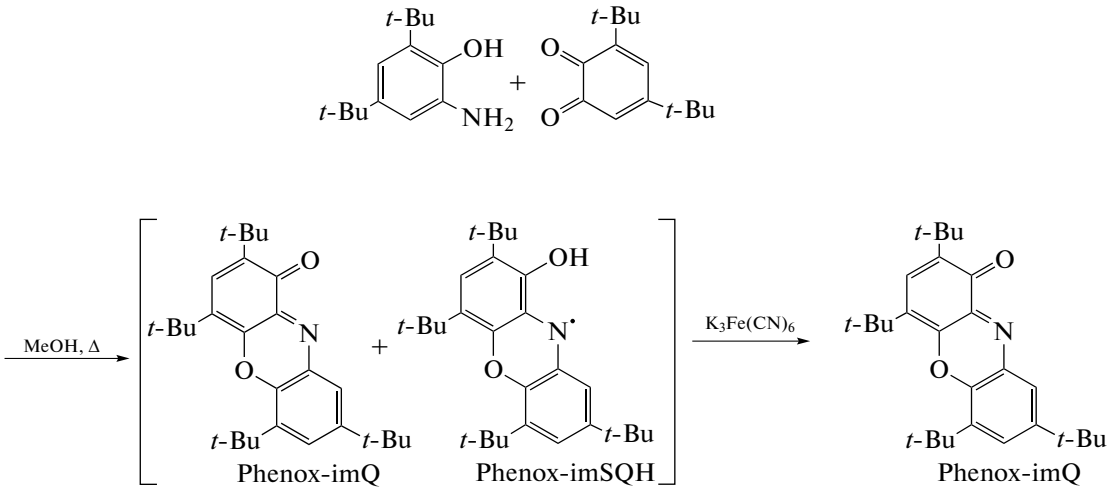

Scheme 1.

The synthesized phenox-imQ ligand is reduced in stages with metallic sodium excess in THF to form the mono- and disodium salts with a change in the color of the reaction mixture from blue to brown (phenox-imSQNa) and further to yellow (phenox-APNa$_2$), respectively. The exchange reaction between the monosodium salt of the ligand and tin organohalides was used to synthesize paramagnetic tin(IV) complexes. The reaction of phenox-imSQNa with R_2SnCl_2 (R = Me, Et, *t*-Bu, and Ph) and Ph_3SnCl in a THF solution ceases within several minutes at room temperature. The reaction mixture turns vinous-red, which is characteristic of the radical-anionic form of the phenoxazinone ligand in the tin(IV) complexes. Complexes **I**–**V** were isolated after crystallization from the reaction mixtures in high yields exceeding 75%. The synthesized compounds are paramagnetic in the crystalline state and in solution and stable towards air oxygen and moisture (Scheme 2).

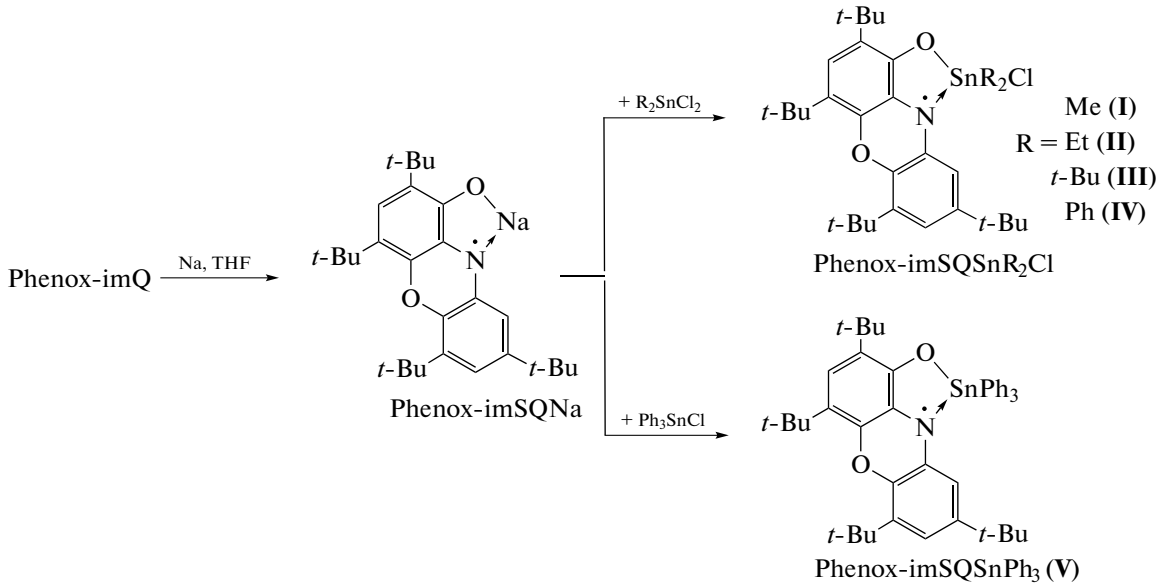

Scheme 2.

Unfortunately, attempts to obtain single crystals of complexes **I**–**V** suitable for XRD were unsuccessful. In order to determine the molecular structures and spin density distribution in the studied compounds, we performed the DFT quantum-chemical calculations (B3LYP/dgdzvp). According to the calculations, the coordination environment of the tin ion in complexes **I**–**V** is a distorted trigonal bipyramid. The structures of the series of complexes were considered in more detail using compound **II** as an example (Fig. 1). The

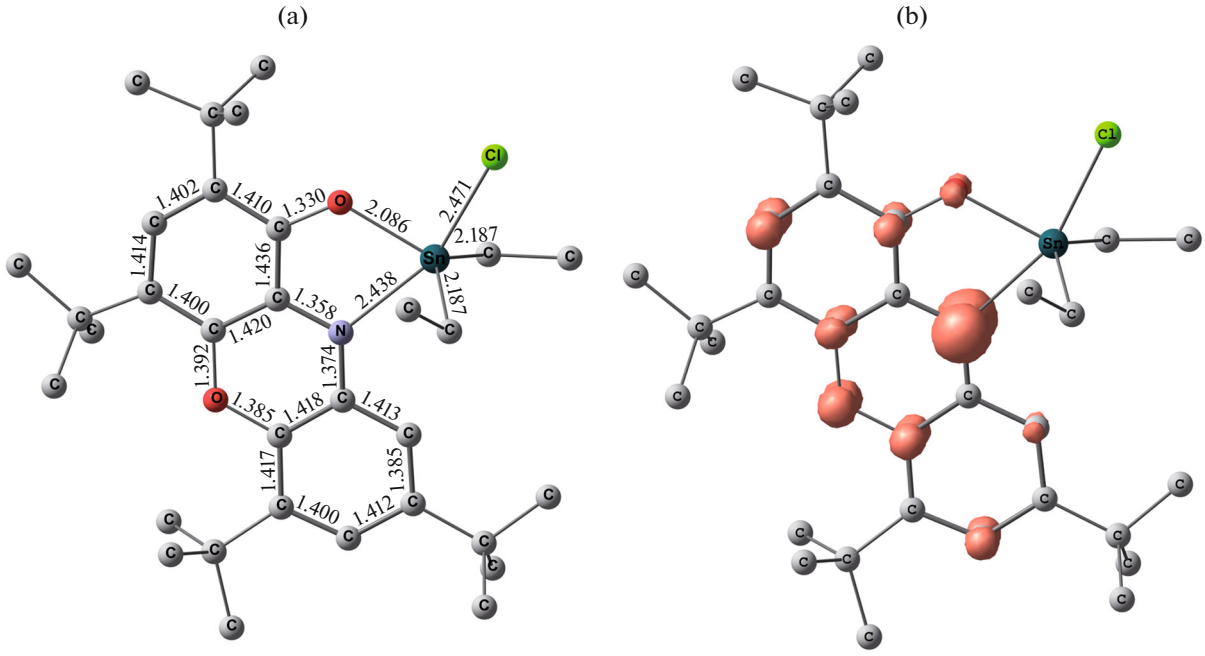

Fig. 1. (a) Optimized geometry of complex **II** (DFT B3LYP/dgdzvp) and (b) spin density distribution in complex **II**. Hydrogen atoms are omitted, and bond lengths are presented in Å.

nitrogen N and halogen Cl atoms occupy the vertices of the bipyramid, whereas the oxygen O atom and carbon atoms of the alkyl substituents form its base. The chlorine atom lies in the plane of the phenoxazinone ligand. The bond lengths in the redox-active ligand are in the range characteristic of the radical-anionic state of phenox-imSQ [35, 36]. A significant difference in the Sn–O (2.086 Å) and Sn–N (2.437 Å) bond lengths should be mentioned, which distinguishes this case from earlier studied tin(IV) *o*-iminosemiquinolates in which the metal–nitrogen and metal–oxygen distances are comparable [37, 38]. Comparing the data obtained, it can be concluded that the character of radical anion binding with the metallocenter can be described as "tin phenolate" additionally coordinated by the nitrogen-centered radical rather than tin "*o*-iminosemiquinolate." A similar coordination mode is demonstrated by the mercury(II) *o*-iminosemiquinone derivatives [39]. An analysis of the spin density distribution shows that the spin density is predominantly (38%) concentrated on the nitrogen atom of the phenoxazinone ligand, whereas the spin density on the tin and chlorine atoms is less than 1%.

All compounds are characterized by the well resolved EPR spectra in the solution. The spectral parameters of the studied complexes **I**–**V** are presented in Table 1. Since the spectra are close in parameters, the EPR spectrum of complex **II** is presented in Fig. 2 as an example. The spectrum represents a triplet (1 : 1 : 1) of doublets (1 : 1) of doublets (1 : 1) of doublets (1 : 1). The hyperfine structure of the spectrum is caused by the interaction of a unpaired electron with three nonequivalent magnetic nuclei of the ^{1}H hydrogen atom (99.98%, $I = 1/2$, $\mu_N = 2.7928$) and one ^{14}N nitrogen atom (99.63%, $I = 1$, $\mu_N = 0.4037$). In addition, the satellite splitting on the magnetic ^{117}Sn (7.68%, $I = 1/2$, $\mu_N = 1.000$) and ^{119}Sn (8.58%, $I = 1/2$, $\mu_N = 1.046$) tin isotopes is observed (Fig. 2). The HFC constants were assigned to the protons in positions 3, 7, and 9 on the basis of the spin density distribution obtained by the DFT calculation results. The absence of the HFC of the unpaired electron with the ^{35}Cl and ^{37}Cl magnetic isotopes correlate well with calculated data, according to which the halogen atom lies in the ligand plane and has no spin density.

The arrangement of the halogen in the plane of the paramagnetic ligand was observed earlier in related pentacoordinate *N*-aryl-substituted *o*-iminosemiquinolates of tin(IV) diorganohalides [23, 24]. However, the latter differ substantially from compounds **I**–**IV** in the formation of the coordination polyhedron. The apical positions of the trigonal bipyramid in the complexes of the $imSQSnR_2Cl$ type, where imSQ is the 4,6-di-*tert*-butyl-*N*-aryl-*o*-iminoquinone radical anion (R is Alk and Ar), are occupied by the halogen and oxygen atoms of the paramagnetic ligand, and the nitrogen atom lies in the equatorial plane [23, 24]. On the contrary, according to the quantum-chemical calculations, the geometry of compound **II** is characterized by the apical arrangement of the nitrogen atom in the trigonal bipyramid. The configuration with nitrogen in the equatorial plane of the trigonal bipyramid also has a minimum on the potential energy surface for

Table 1. Parameters of the isotropic EPR spectra (G) for complexes **I**–**VIII**

Complex	a_i(H(7))	a_i(H(9))	a_i(H(3))	a_i(^{14}N)	a_i(^{117}Sn,^{119}Sn)	g_i
I	2.16	3.28	4.11	7.93	6.50; 6.80	2.0030
II	2.18	3.35	4.15	7.98	7.68; 8.04	2.0031
III	2.15	3.31	4.13	7.89	5.26; 5.51	2.0031
IV	2.11	3.30	4.13	7.95	4.83; 5.05	2.0030
V	2.31	3.40	4.19	7.98	1.73; 1.81	2.0029
VII	2.18	3.35	4.20	7.97	8.41; 8.79	2.0032
VIII	2.20	3.34	4.25	7.97	6.12; 6.40	2.0033

compound **II**. However, this configuration is destabilized by 5 kcal/mol compared to that presented in Fig. 1. The presence of the nitrogen atom of the *o*-iminosemiquinolate radical anion in the apical position in complexes **I**–**IV** is accompanied by a decrease in the HFC constants with the ^{117}Sn and ^{119}Sn magnetic isotopes in the EPR spectra of the phenoxazinone derivatives by 5–10 times compared to imSQSnR$_2$Cl. In the case of *N*-aryl-substituted tin(IV) *o*-iminosemiquinolates, the characteristic value of the HFC constants ranges from 40 to 50 G [23, 24], whereas for the synthesized phenox-imSQSnR$_2$Cl complexes (**I**–**IV**) this range is 5–8 G (Table 1). Taking into account that the spin density in the phenoxazinone radical anion is predominantly concentrated on the nitrogen atom, the spin σ–π polarization of the N–Sn bond will significantly introduce to the HFC constants on the magnetic metal isotopes. It is known [40] that an increase in the HFC constants in the EPR spectra is observed upon the interaction of the orbital occupied by a unpaired electron with the *s* orbital of the element having the nonzero density on the element core. It can be expected that for the sp^3d hybridization in the trigonal bipyramid the contribution of the *s* orbital of the metal to the formation of the hybrid atomic orbital providing binding with the equatorial substituents in the coordination sphere of tin(IV) should be much higher than that for the apical directions, which are, most likely, of the p_z,d_{z^2} character [41]. Thus, the migration of the nitrogen atom of the radical-anionic ligand from the equatorial to an axial position is the main reason for to a sharp decrease in the HFC constants with the ^{117}Sn and ^{119}Sn magnetic isotopes in paramagnetic complexes **I**–**IV** compared to *N*-substituted tin(IV) *o*-iminosemiquinolates. Another characteristic feature observed in the EPR spectra of these pentacoordinate complexes of diorganotin(IV) is the dependence of the HFC constant with the ^{117,119}Sn magnetic isotopes on the nature of the hydrocarbon substituents on the metal. For example, an increase in the HFC constant with an increase in the branching of the alkyl substituents is observed for the pentacoordinate complexes of diorganotin(IV) containing the nitrogen atom in the equatorial plane [23, 42]. In this work, we observe an opposite dependence for derivatives **I**–**III**. This observation is due, most likely, to a change in the character of the atomic orbital of the metal responsible for binding with the nitrogen center of the radical anion.

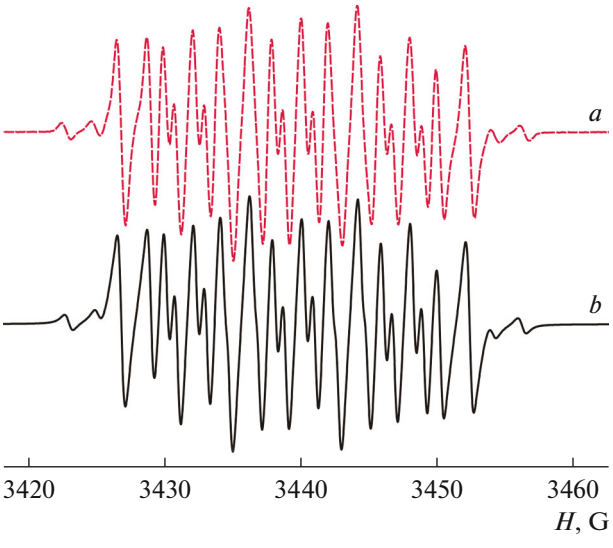

Fig. 2. Isotropic EPR spectrum of the phenox-imSQSnEt$_2$Cl complex (**II**) in THF at $T = 298$ K: (*a*) theoretical and (*b*) experimental spectra.

It should be mentioned that for complex **V** containing three phenyl substituents at the tin atom the HFC constant on the magnetic tin isotopes decreases compared to those for complexes **I**–**IV** and is equal to 1.75 G. This fact can be due to steric hindrances induced by three phenyl groups at the tin atom, which results in the elongation of the distance between the metallocenter and redox-active ligand. A similar tendency was also observed in the earlier studied tin *o*-iminosemiquinolates ongoing from imSQSnR$_2$Cl to imSQSnR$_3$ [14]. Triphenyl complex **V** was generated in a solution previously [43] but was not isolated in the individual state and only studied by EPR spectrocopy in solution.

As described above, phenox-imQ can be reduced by two equivalents of metallic sodium to form disodium salt phenox-APNa$_2$. The reaction of the synthesized salt with Et_2SnCl_2 in a ratio of 1 : 1 in a THF solution afforded the diamagnetic tin(IV) complex: phenox-APSnEt$_2$(THF) (**VI**) (Scheme 3).

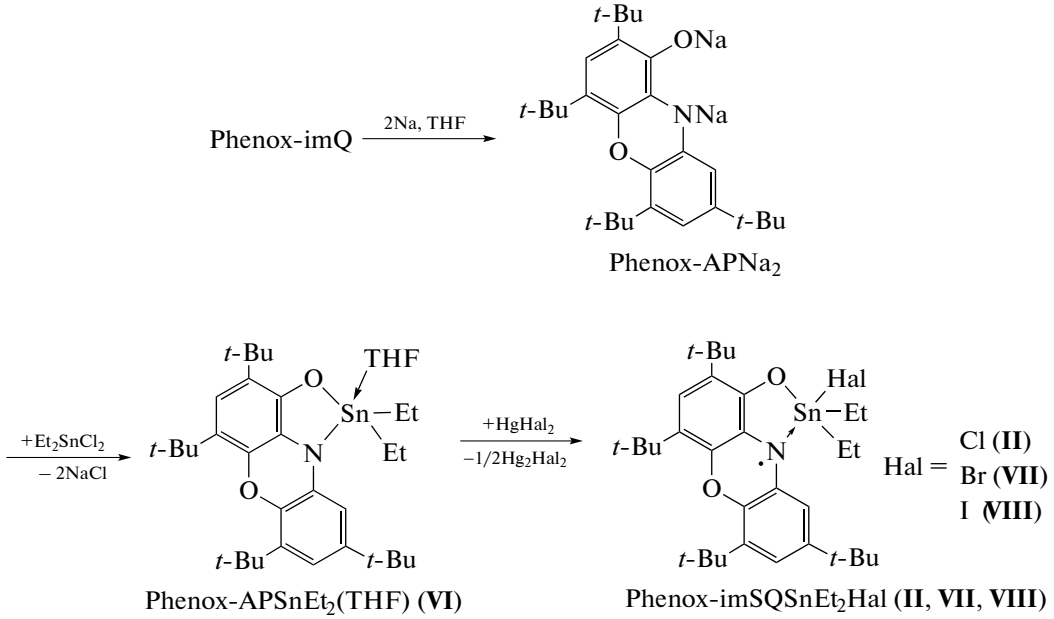

Scheme 3.

The color of the reaction mixture changed from yellow to intensive orange during the reaction. Complex **VI** was found to be sensitive to air oxygen and moisture. The crystals suitable for XRD were isolated from a THF solution during the slow evaporation of the solvent. The crystal structure of compound **VI** is presented in Fig. 3. Selected bond lengths and angles are given in Table 2. According to the XRD data, complex **VI** crystallizes in the monoclinic space group $P2_1/n$. The independent part of the crystalline cell contains one complex molecule in the common position and one solvate THF molecule. Thus, complex **VI** crystallizes as solvate **VI** · THF. The coordination environment of the tin atom in complex **VI** · THF represents a distorted tetragonal pyramid, whose vertex is occupied by the C(29) carbon atom, and the square base is formed by the C(31) carbon, O(1) oxygen (O(THF)), and N(1) nitrogen atoms. The geometric parameter τ is used for an analysis of the coordination sphere of the pentacoordinate complexes. The value of τ is equal to zero in an ideal square pyramid and to 1 in an ideal trigonal bipyramid [44]. In complex **VI** · THF $\tau = 0.32$, which corresponds to a strongly distorted tetragonal pyramidal geometry of the coordination environment of the tin atom. Remarkably, the structure of the closest analog of compound **VI** among the pentacoordinate *o*-iminoquinone derivatives, *o*-amidophenolate complex ^{dipp}APSnEt$_2$THF [45], is much closer to a trigonal bipyramid with $\tau = 0.75$. Thus, the transition from the 4,6-di-*tert*-butyl-*N*-aryl-*o*-iminobenzoquinone derivatives to the phenox-imQ-based compounds with similar structures is accompanied by a substantial change in the type of coordination geometry.

The bond lengths in the six-membered carbon rings (see Table 2) are close to aromatic bond lengths (~1.40 Å), which along with the characteristic C(1)–O(1) (1.368(2) Å) and C–N (1.388(2), 1.398(2) Å) distances [46, 47] unambiguously indicate the dianionic state of the redox-active ligand in complex **VI** · THF. The Sn–O(1) (2.018(2) Å) and Sn–N(1) (2.103(2) Å) bond lengths are shorter than the sum of the van der Waals radii of the corresponding elements [48] and indicate the covalent character of the interaction of the phenoxazinone ligand dianion with the metallocenter. It should be mentioned that the synthesized compound is the first structurally characterized compound containing the phenox-imQ ligand in the dianionic form. The published data on the structures of the metal complexes containing this ligand in the neutral [49, 50] and radical-anionic forms [35, 36, 51–54] are available.

The reactions of complex **VI** with mercury halides ($HgCl_2$, $HgBr_2$, and HgI_2) were carried out under the EPR experimental conditions in order to find a possibility for the oxidation of the dianionic ligand in the complex under study. As shown previously, the chosen reagents are convenient one-electron oxidants that allow one to synthesize the radical derivatives in the reactions with the catecholate, *o*-amidophenolate,

and diamine metal complexes [55–57]. The products of these reactions were studied by solution EPR spectroscopy in situ and were not isolated in the individual state. The interaction of solutions of complex **VI** with $HgHal_2$ is accompanied by a change in the color of the solution from orange to vinous-red, and the signals similar to those considered above for complexes **I**–**V** appear in the EPR spectra. The EPR spectral parameters are presented in Table 1. The spectrum of the reaction product with mercury(II) chloride is identical to that for complex **II**. An analysis of the parameters of the observed EPR spectra suggests that the paramagnetic derivatives phenox-im$SQSnEt_2Hal$ (**II**, **VII**, and **VIII**) are formed during oxidation (Scheme 3), and their structures are similar to that described above. It should be mentioned that the change in the HFC constants of the unpaired electron with the $^{117,119}Sn$ magnetic isotopes induced by the replacement of halogen cannot be described by any unambiguous dependence. The highest constants (see Table 1) are observed for the bromine derivative. Probably, the absence of a correlation between the HFC constants with $^{117,119}Sn$ in the Cl–Br–I series can be induced by the action of several factors (steric and electronic effects, change in the contributions of atomic orbitals to hybridization) that exert different effects on the measured parameter.

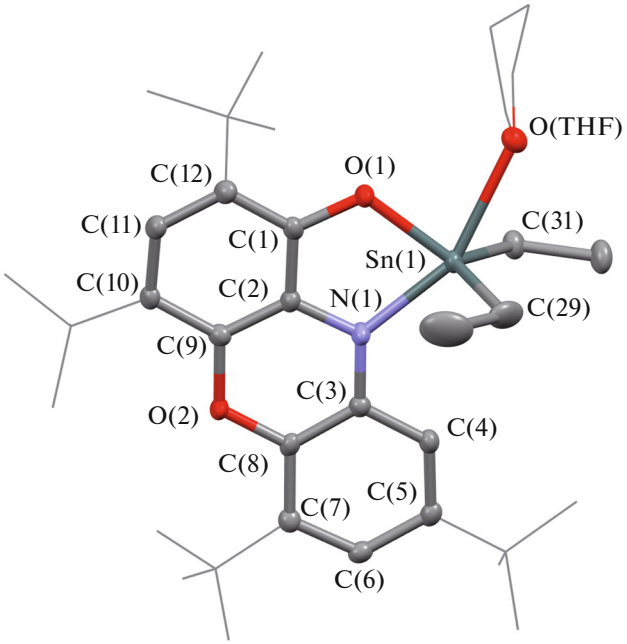

Fig. 3. Molecular structure of complex **VI**. Thermal ellipsoids for the key atoms are given with 50% probability. Hydrogen atoms are omitted for clarity.

It is shown in the work that the *o*-iminosemiquinone radical-anionic ligands can act as fairly informative spin labels that make it possible to study the molecular and electronic structures of organoelement compounds in a solution. They have a substantial advantage over *o*-semiquinones traditionally used for this purpose, since they induce no elimination of carbanionic substituents at the metal. It is demonstrated for the organotin compounds that the EPR spectral parameters observed for their *o*-iminosemiquinone derivatives are very sensitive to the structure of the

Table 2. Selected bond lengths (Å) and angles (deg) in complex **VI** · THF

Bond	*d*, Å	Bond	*d*, Å
Sn(1)–O(1)	2.018(2)	O(2)–C(9)	1.408(2)
Sn(1)–N(1)	2.103(2)	C(2)–C(9)	1.393(2)
Sn(1)–C(31)	2.136(2)	C(3)–C(4)	1.402(2)
Sn(1)–C(29)	2.137(2)	C(3)–C(8)	1.405(2)
Sn(1)–O(THF)	2.438(2)	C(4)–C(5)	1.392(2)
O(1)–C(1)	1.368(2)	C(5)–C(6)	1.394(2)
N(1)–C(3)	1.388(2)	C(6)–C(7)	1.404(2)
N(1)–C(2)	1.398(2)	C(7)–C(8)	1.409(2)
C(1)–C(12)	1.399(2)	C(9)–C(10)	1.406(2)
C(1)–C(2)	1.406(2)	C(10)–C(11)	1.406(2)
O(2)–C(8)	1.403(2)	C(11)–C(12)	1.396(2)
Angle	ω, deg	Angle	ω, deg
O(1)Sn(1)N(1)	80.05(5)	N(1)Sn(1)C(31)	103.77(7)
C(31)Sn(1)C(29)	123.02(9)	O(1)Sn(1)C(29)	108.22(8)
O(1)Sn(1)O(3)	76.19(5)	N(1)Sn(1)C(29)	105.02(8)
N(1)Sn(1)O(3)	155.25(5)	O(1)Sn(1)O(3)	76.19(5)
O(1)Sn(1)C(31)	124.54(7)		

coordination polyhedron, nature of alkyl substituents at the metal atom, and the number of alkyl substituents, which affects the values of the HFC constants on the magnetic isotopes of the metal.

ACKNOWLEDGMENTS

The studies were carried out in terms of state assignment using the equipment of the Analytical Center for Collective Use at the Razuvaev Institute of Organometallic Chemistry (Russian Academy of Sciences)

FUNDING

This work was supported by the federal target program "Research and Design on Priority Directions of Development of Scientific Technological Complex of Russia for 2014–2020" (project no. RFMEFI62120X0040).

CONFLICT OF INTEREST

The authors declare that they have no conflicts of interest.

REFERENCES

1. Kabachnik, M.I., *Pure Appl. Chem.*, 1980, vol. 52, p. 859.
2. Broere, D.L.J., Plessius, R., and van der Vlugt, J.I., *Chem. Soc. Rev.*, 2015, vol. 44, p. 6886.
3. Tezgerevska, T., Alley, K.G., and Boskovic, C., *Coord. Chem. Rev.*, 2014, vol. 268, p. 23.
4. Jacquet, J., Cheaib, K., Ren, Y., et al., *Chem.-Eur. J.*, 2017, vol. 23, p. 1530.
5. Kaim, W. and Paretzki, A., *Coord. Chem. Rev.*, 2017, vol. 344, p. 345.
6. van der Vlugt, J.I., *Chem.-Eur. J.*, 2019, vol. 25, p. 2651.
7. Khan, F.F., Chowdhury, A.D., and Lahiri, G.K., *Eur. J. Inorg. Chem.*, 2020, p. 1138.
8. Abakumov, G.A., Piskunov, A.V., Cherkasov, V.K., et al., *Russ. Chem. Rev.*, 2018, vol. 87, p. 393.
9. Poddel'sky, A.I., Cherkasov, V.K., and Abakumov, G.A., *Coord. Chem. Rev.*, 2009, vol. 253, p. 291.
10. Chirik, P.J. and Wieghardt, K., *Science*, 2010, vol. 327, p. 794.
11. Kaim, W. and Schwederski, B., *Coord. Chem. Rev.*, 2010, vol. 254, p. 1580.
12. Kozhanov, K.A., Bubnov, M.P., Cherkasov, V.K., et al., *Dalton Trans.*, 2004, p. 2957.
13. Kozhanov, K.A., Bubnov, M.P., Cherkasov, V.K., et al., *Dalton Trans.*, 2008, p. 2849.
14. Bubnov, M.P., Teplova, I.A., Kozhanov, K.A., et al., *J. Magn. Reson.*, 2011, vol. 209, p. 149.
15. Kozhanov, K.A., Bubnov, M.P., Abakumov, G.A., and Cherkasov, V.K., *J. Magn. Reson.*, 2012, vol. 225, p. 62.
16. Kozhanov, K.A., Bubnov, M.P., Teplova, I.A., et al., *J. Mol. Struct.*, 2017, vol. 1147, p. 541.
17. Bubnov, M.P., Kozhanov, K.A., Skorodumova, N.A., et al., *J. Mol. Struct.*, 2019, vol. 1180, p. 878.
18. Chegerev, M.G. and Piskunov, A.V., *Russ. J. Coord. Chem.*, 2018, vol. 44, p. 258. https://doi.org/10.1134/S1070328418040036
19. Ershova, I.V. and Piskunov, A.V., *Russ. J. Coord. Chem.*, 2020, vol. 46, p. 154. https://doi.org/10.1134/S1070328420030021
20. Razuvaev, G.A., Tsarjapkin, V.A., Gorbunova, L.V., et al., *J. Organomet. Chem.*, 1979, vol. 174, p. 475.
21. Prokof'ev, A.I., Pombrik, S.I., Kasymbekova, Z.K., et al., *Russ. Chem. Bull.*, 1982, vol. 31, p. 482.
22. Razuvaev, G.A., Abakumov, G.A., Bayushkin, P.Y., et al., *Russ. Chem. Bull.,* 1984, vol. 33, p. 1915.
23. Piskunov, A.V., Meshcheryakova, I.N., Baranov, E.V., et al., *Russ. Chem. Bull.,* 2010, vol. 59, p. 361.
24. Piskunov, A.V., Chegerev, M.G., Vaganova, L.B., et al., *Russ. J. Coord. Chem.*, 2015, vol. 41, p. 428. https://doi.org/10.1134/s1070328415070076
25. Gordon, A. and Ford, R., *The Chemist's Companion: A Handbook of Practical Data, Techniques, and References*, New York: Wiley, 1972.
26. Stoll, S. and Schweiger, A.J., *J. Magn. Reson.*, 2006, vol. 178, p. 42.
27. Ivakhnenko, E.P., Karsanov, I.V., Khandrakova, V.S., et al., *Russ. Chem. Bull.,* 1986, vol. 35, p. 2526.
28. Vol'eva, V.B., Prokofeva, T.I., Prokofev, A.I., et al., *Russ. Chem. Bull.,* 1995, vol. 44, p. 1720.
29. Stegmann, H.B. and Scheffler, K., *Chem. Ber.*, 1968, vol. 101, p. 262.
30. Frisch, M.J., Trucks, G.W., Schlegel, H.B., et al., *Gaussian 09, Revision D.01*, Wallingford (CT, USA): Gaussian, Inc., 2013.
31. Becke, A.D., *J. Chem. Phys.*, 1993, vol. 98, p. 5648.
32. *Rigaku Oxford Diffraction. CrysAlisPro Software System. Version 1.171.35.19*, Wroclaw: Rigaku Corporation, 2011.
33. Sheldrick, G.M., *Acta Crystallogr., Sect. C*: *Struct. Chem.*, 2015, vol. 71, p. 3.
34. Spek, A.L., *Acta Crystallogr., Sect. C*: *Struct. Chem.*, 2015, vol. 71, p. 9.
35. Romanenko, G.V., Ivakhnenko, E.P., Minkin, V.I., et al., *Inorg. Chim. Acta*, 2014, vol. 418, p. 66.
36. Ivakhnenko, E.P., Starikov, A.G., Lyssenko, K.A., et al., *Inorg. Chim. Acta*, 2014, vol. 410, p. 144.
37. Piskunov, A.V., Mescheryakova, I.N., Fukin, G.K., et al., *Heteroatom Chem.*, 2009, vol. 20, p. 332.
38. Piskunov, A.V., Meshcheryakova, I.N., Piskunova, M.S., et al., *J. Mol. Struct.*, 2019, vol. 1195, p. 417.
39. Piskunov, A.V., Meshcheryakova, I.N., Smolyaninov, I.V., et al., *Russ. Chem. Bull.,* 2013, vol. 62, p. 147.
40. Abakumov, G.A., Cherkasov, V.K., Piskunov, A.V., et al., *Russ. Chem. Bull.,* 2006, vol. 55, p. 1146.
41. Gillespie, R.J., *J. Chem. Soc.*, 1963, p. 4672.
42. Piskunov, A.V., Sukhoshkina, O.Y., and Smolyaninov, I.V., *Russ. J. Gen. Chem.*, 2010, vol. 80, p. 790.
43. Karsanov, I.V., Ivakhnenko, E.P., Khandkarova, V.S., et al., *Russ. Chem. Bull.,* 1987, vol. 36, p. 56.
44. Addison, A.W., Rao, T.N., Reedijk, J., et al., *Dalton Trans.*, 1984, p. 1349.
45. Piskunov, A.V., Aivaz'yan, I.A., Abakumov, G.A., et al., *Russ. Chem. Bull.,* 2007, vol. 56, p. 261.

46. Brown, S.N., *Inorg. Chem.*, 2012, vol. 51, p. 1251.
47. Chegerev, M.G., Piskunov, A.V., Starikova, A.A., et al., *Eur. J. Inorg. Chem.*, 2018, p. 1087.
48. Batsanov, S.S., *Russ. J. Inorg. Chem.*, 1991, vol. 36, p. 1694.
49. Ivakhnenko, E.P., Koshchienko, Y.V., Chernyshev, A.V., et al., *Russ. J. Gen. Chem.*, 2016, vol. 86, p. 1664.
50. Ivakhnenko, E.P., Koshchienko, Yu.V., Knyazev, P.A., et al., *Russ. J. Coord. Chem.*, 2016, vol. 42, p. 509. https://doi.org/10.1134/s1070328416040011
51. Antipin, M.Yu., Ivakhnenko, E.P., Koshchienko, Yu.V., et al., *Russ. Chem. Bull.,* 2013, vol. 62, p. 1744.
52. Speier, G., Whalen, A.M., Csihony, J., and Pierpont, C.G., *Inorg. Chem.*, 1995, vol. 34, p. 1355.
53. Bhattacharya, S. and Pierpont, C.G., *Inorg. Chem.*, 1994, vol. 33, p. 6038.
54. Whalen, A.M., Bhattacharya, S., and Pierpont, C.G., *Inorg. Chem.*, 1994, vol. 33, p. 347.
55. Piskunov, A.V., Tsys, K.V., Chegerev, M.G., et al., *Russ. J. Coord. Chem.*, 2019, vol. 45, p. 626. https://doi.org/10.1134/s1070328419090069
56. Tsys, K.V., Chegerev, M.G., Fukin, G.K., et al., *Mendeleev Commun.*, 2018, vol. 28, p. 527.
57. Abakumov, G.A., Cherkasov, V.K., Piskunov, A.V., et al., *Dokl. Chem.*, 2005, vol. 404, p. 189.

Translated by E. Yablonskaya